ACS APPLIED MATERIALS & INTERFACES

RESEARCH ARTICLE

www.acsami.org

Rapid Fabrication of Large-Area, Corrosion-Resistant Superhydrophobic Mg Alloy Surfaces

Wenji Xu,* Jinlong Song, Jing Sun, Yao Lu, and Ziyuan Yu

School of Mechanical Engineering, Dalian University of Technology, Dalian 116024, People's Republic of China

ABSTRACT: A superhydrophobic magnesium (Mg) alloy surface was successfully fabricated via a facile electrochemical machining process, and subsequently covered with a fluoroalkylsilane (FAS) film. The surface morphologies and chemical compositions were investigated using a scanning electron microscope (SEM) equipped with an energy-dispersive spectroscopy (EDS) and a Fourier-transform infrared spectrophotometer (FTIR). The results show hierarchal rough structures and an FAS film with a low surface energy on the Mg alloy surfaces, which confers good superhydrophobicity with a water contact angle of 165.2° and a water tilting angle of approximately 2°. The processing conditions, such as the processing time and removal rate per unit area at a constant removal mass per unit area, were investigated to determine their effects on the superhydrophobicity. Interestingly, when the removal mass per unit area is constant at approximately 11.10 mg/cm^2, the superhydrophobicity does not change with the removal rate per unit area. Therefore, a superhydrophobic Mg alloy surface can be rapidly fabricated based on this property. A large-area superhydrophobic Mg alloy surface was also fabricated for the first time using a small-area moving cathode. The corrosion resistance and durability of the superhydrophobic surfaces were also examined.

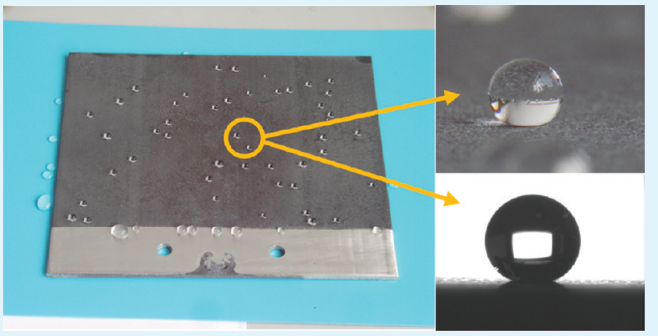

KEYWORDS: superhydrophobic surface, large area, corrosion resistance, electrochemical machining, Mg alloy

1. INTRODUCTION

Magnesium (Mg) alloys are the lightest metal structure materials among the practical metals, and their specific gravity is approximately 2/3 and 1/4 that of aluminum (Al) and steel, respectively. In the last decades, Mg alloys have been utilized in several industrial fields for different applications because of their low specific gravity, high strength-to-weight ratio, and good shock adsorption capacity.[1] Two important fields that use of Mg alloys are the automobile and aerospace industries, in which a reduction in the total weight could lead to fuel saving or load increase. However, they have a serious drawback: extremely low corrosion resistance.[2,3] Given that Mg is a very reactive metal and readily corrodes in some environments, Mg alloys commonly serve as sacrificial anodes.[4] This corrosion behavior prevents the large-scale application of Mg alloys.[5] Various methods have been developed to improve their corrosion resistance. In recent years, superhydrophobic surfaces with a water contact angle larger than 150° and a tilting angle smaller than 10° have been proven effective in preventing Mg alloy corrosion.[2,6−14]

The superhydrophobic surface, which was first observed on lotus leaves, has inspired researchers around the world because of its importance in fundamental research as well as its potential industrial use, such as for self-cleaning, friction reduction, anticing, and corrosion resistance. The corrosion resistance mechanism of superhydrophobic surfaces proceeds as follows: when immersed in a corrosion solution, superhydrophobic surfaces composed of hierarchal rough structures can easily trap a large amount of air within the valleys between the rough structures. These "air valleys" then prevent the migration of corrosive ions. In recent years, researchers have conducted extensive studies on the corrosion resistance of the superhydrophobic surfaces of Al, copper (Cu), steel, and Mg substrates.[15−18]

Currently, a number of fabrication methods for superhydrophobic surfaces on Mg and its alloys have been reported. In 2007, Liang et al. first reported the fabrication of a stable biomimetic superhydrophobic surface on Mg alloys via microarc oxidation and chemical modification.[19] However, the superhydrophobicity was not sufficient, with a water contact angle only slightly larger than 150° and a water tilting angle only slightly smaller than 8°. In 2008, Jiang et al. fabricated a superhydrophobic surface on Mg−Li alloys via chemical etching, followed by modification with an ultrathin fluoroalkylsilane (FAS) coating.[20] However, this method has low processing efficiency and requires a long processing time (approximately 14 h). In 2010, Wang et al. fabricated a superhydrophobic surface on a pure Mg substrate via wet chemical etching in a 1% H_2SO_4 aqueous solution for 4 min and in a 20% H_2O_2 aqueous solution for 150 s, followed by modification with stearic acid;[10] Yin et al. obtained a superhydrophobic surface on AZ31 Mg alloys via immersion using an aqueous solution of nitric acid (HNO_3) and copper nitrate trihydrate [$Cu(NO_3)_2 \cdot 3H_2O$], followed by modification with triethoxyoctylsilane.[9] However, because of the use of strong acids, the methods of Wang and Yin are hazardous for operators

Received: August 6, 2011
Accepted: October 18, 2011
Published: October 18, 2011

dx.doi.org/10.1021/am2010527 | ACS Appl. Mater. Interfaces 2011, 3, 4404–4414

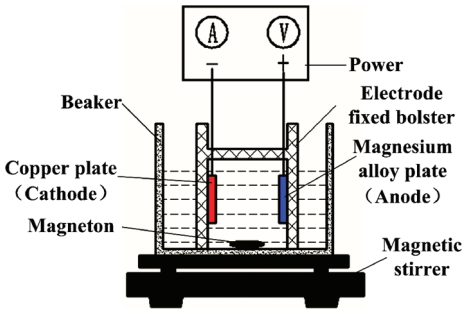

Figure 1. Schematic representation of the experimental setup.

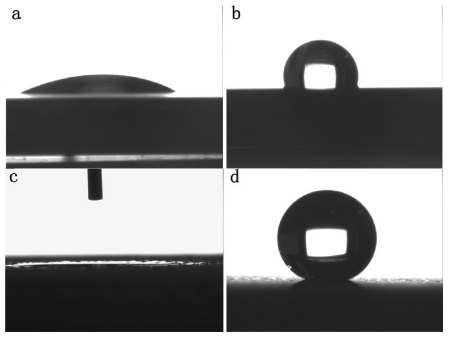

Figure 2. Images of the water contact angles on the Mg alloy surfaces: (a) untreated Mg alloy surfaces, (b) Mg alloy surfaces treated with FAS, (c) superhydrophilic Mg alloy surfaces treated via electrochemical machining at the 200 mA/cm^2 processing current density and 5 min processing time without FAS modification, and (d) superhydrophobic Mg alloy surfaces treated via electrochemical machining and FAS modification.

and could pollute the environment. In the same year, Ishizaki et al. fabricated a superhydrophobic surface on AZ31 Mg alloys coated with a cerium oxide film via an immersion process in an acidic solution containing 0.05 mol/L cerium nitrate hexahydrate [$Ce(NO_3)_3 \cdot 6H_2O$].[2] Despite comparing with the strong acids, the use of cerium nitrate does not present obvious danger; however, it is a burning-rate accelerator and could irritate the skin and accumulate in groundwater. In 2011, Wang et al. constructed superhydrophobic hydromagnesite films on Mg alloys via immersion in a urea aqueous solution at 150 °C, followed by modification and annealing processes using FAS.[7] However, this procedure also requires a long processing time (26 h). Ishizaki et al. suggested a new hot-water immersion method to fabricate superhydrophobic surfaces,[6] but the processing time lasts several hours. In addition, all the aforementioned methods did not fabricate large-area superhydrophobic surfaces. Therefore, a highly effective, environmentally friendly, safe, nontoxic method suitable for large-area fabrication is needed.

In the current paper, we report a simple electrochemical machining method using a relatively nonpoisonous neutral sodium chloride (NaCl) aqueous solution for the fabrication of a superhydrophobic surface on AZ61 Mg alloys at the room temperature. In the first step, the hierarchical rough structures were fabricated on the Mg alloy surfaces via electrochemical machining in a 0.2 mol/L NaCl aqueous solution. In the second step, the self-assembly of the hydrophobic FAS film on the Mg alloy surfaces was induced by immersing the electrochemically machined Mg alloys in an FAS ethanol solution. Electrochemical machining using a small-area moving cathode, which has been widely used in the military industry to process the large-scale work pieces, was introduced in the present study to fabricate large-area superhydrophobic Mg alloy surfaces for the first time.

2. EXPERIMENTAL SECTION

2.1. Materials. Commercially available Mg alloy AZ61 plates (Dongguan Jiahao Die Materials Co., PR China; composition: Al of 6.29 wt %, Zn of 0.98%, M_n of 0.37%, with the balance being Mg) were used as the substrates. A Cu plate (99.9% purity) was obtained from Tianjin Kermel Chemical Reagent Co., China. FAS [tridecafluoroctyltriethoxysilane, $C_8F_{13}H_4Si(OCH_2CH_3)_3$] was obtained from Degussa Co., Germany. Analytical-grade NaCl was obtained from Shanghai Chemical ReagentCo., China.

2.2. Fabrication of Superhydrophobic Surfaces. Prior to electrochemical machining, the Mg alloys (30 mm ×20 mm ×2 mm) were polished mechanically using a 1500# metallographic abrasive paper to remove the impurities and the oxide/hydroxide layer on the surfaces. The Mg alloys were then sequentially cleaned with alcohol and deionized water via ultrasonication. After being dried, the anodic Mg alloy plate and the cathodic Cu plate of equal size were separated by a distance of 20 mm. The Mg alloy plates were then electrochemically machined in the 0.2 mol/L NaCl electrolyte at different processing current densities and different processing time. The samples were then ultrasonically rinsed with deionized water and dried. Finally, the as-obtained Mg alloys were immersed in a 1.0 wt % ethanol solution of FAS for 45 min and subsequently heated at 80 °C for 15 min. The schematic representation of the experimental setup is shown in Figure 1.

2.3. Sample Characterization. The surface morphologies and chemical compositions of the obtained samples were investigated using a scanning electron microscope (SEM, JSM-6360LV, Japan) equipped with an energy-dispersive spectropscopy (EDS, INCA Energy, Oxford Ins) and a Fourier-transform infrared spectrophotometer (FTIR, JACSCO, Japan). The surface roughness was measured using a 3D surface profilometer (Model Talysurf CLI2000, UK). The water contact angles were measured at ambient temperature using an optical contact angle meter (Krüss, DSA100, Germany) and the tilting angles were measured using the conventional tilting plate method. Water droplets (5 μL) were carefully dropped onto the surfaces, and the average value of five measurements obtained at different positions in the samples was used as the final contact angle. All electrochemical measurements were performed in 3.5 wt % aqueous solutions of NaCl, Na_2SO_4, $NaClO_3$, and $NaNO_3$ at room temperature using a computer-controlled potentiostat (Princeton Applied Research, VersaSTAT, USA) under open circuit conditions. For these electrochemical measurements, a three-electrode configuration, with a superhydrophobic Mg alloy surface (area, 4 cm^2) as the working electrode, a platinum electrode as the counter electrode, and a saturated calomel electrode (SCE) as the reference electrode, was used. The polarization curves were obtained at a sweep rate of 2 mV/s. The electrochemical impedance spectroscopy (EIS) measurements were conducted in the 100 mHz to 100 kHz frequency range using a 5 mV amplitude perturbation.

3. RESULTS AND DISCUSSION

3.1. Wettability of the Mg Alloy Surfaces. Figure 2 shows the images of the water contact angles on the different types of Mg alloy surfaces, which clearly demonstrate the change in the wettability of the Mg alloy surfaces with the treatment method. The water contact angle of the untreated Mg alloy surfaces is approximately 30.9°, indicating hydrophilicity. After modification with FAS, the water contact angle increases to 106.6°, indicating hydrophobicity. Obviously, FAS has a very low surface energy and can easily decrease the free energy of the Mg alloy

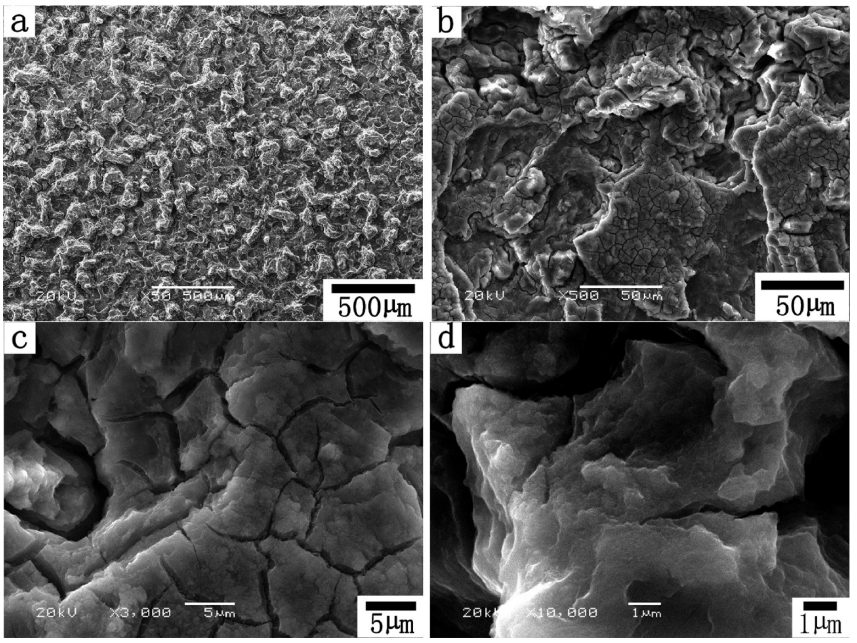

Figure 3. SEM images of the Mg alloy surfaces obtained at the 200 mA/cm^2 processing current density and 5 min processing time: (a) × 50; (b) × 500; (c) × 3000; and (d) × 10000 magnification.

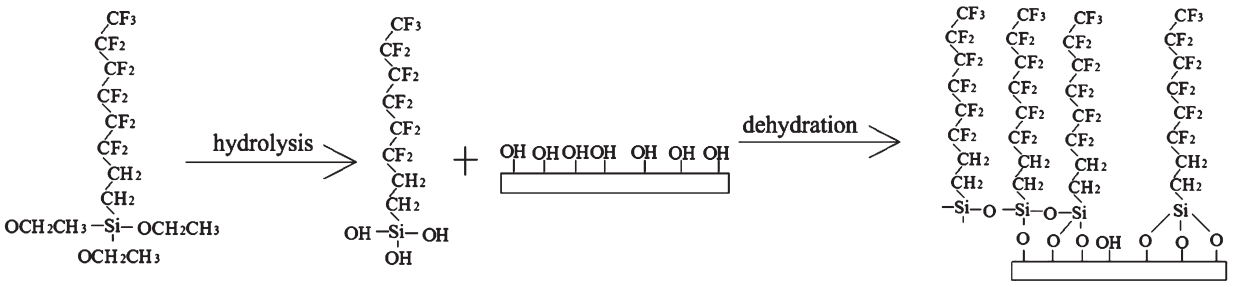

Figure 4. Formation scheme of the self-assembled FAS film on the Mg alloy surfaces.

surfaces. After electrochemical machining at the 200 mA/cm^2 processing current density and 5 min processing time, the Mg alloy surfaces exhibit superhydrophilicity prior to fluorination. The water droplets completely spread on the surfaces at a water contact angle of approximately 0°. Finally, after modification with FAS, the character of the Mg alloy surfaces successfully changes from superhydrophilic to superhydrophobic, with a water contact angle of 165.2° and a water tilting angle of approximately 2°. The results clearly indicate that electrochemical machining and low-surface energy material modification are both important in the fabrication of superhydrophobic Mg alloy surfaces.

3.2. Analysis of the Microstructure and Superhydrophobicity. The SEM images of the Mg alloy surfaces obtained at the 200 mA/cm^2 processing current density and 5 min processing time are shown in Figure 3. The images are shown in different magnifications. The Mg alloy surfaces appear rough after electrochemical machining. Figure 3a shows that the surfaces consist of micrometer-scale pits and protrusions 100 to 250 μm in diameter; Figure 3b shows the SEM image at 500× magnification. Smaller lumplike structures exist in the micrometer-scale pits and protrusions. Figure 3c shows a magnified image of a typical micrometer-scale lump-like structure. Several cracks 1 μm wide are formed on the surfaces of the lump-like structures, with a number of cracks linking and dividing the lumplike structures into block structures 3−10 μm in diameter. The SEM image at 10000× magnification (Figure 3d) shows that the surface of the block structures is not smooth but consists of the nanometer scale cavities and mastoids. Thus, after electrochemical machining, hierarchical rough structures similar to the microstructures of the lotus leaf surface are formed on the Mg alloy surfaces.

The AZ61 Mg alloy is a hydrophilic material with a water contact angle of 30.9°. After acquiring hierarchical rough structures, the Mg alloy surfaces exhibit superhydrophilic properties. This result verifies the assumption proposed by Wenzel that rough surface structures can enhance the hydrophilicity of a given hydrophilic Mg alloy surface.

According to the Wenzel equation[21]

$$\cos \theta_c = r\cos \theta \quad (1)$$

where r is the roughness defined as the ratio between the real and projected solid−liquid contact areas, and $\theta_c$and θ are the contact angles on the rough and smooth surfaces, respectively. Given that θ_c =0° and θ = 30.9°, r is estimated as 1.17 according to eq 1. Thus, when a water droplet is placed on the superhydrophilic

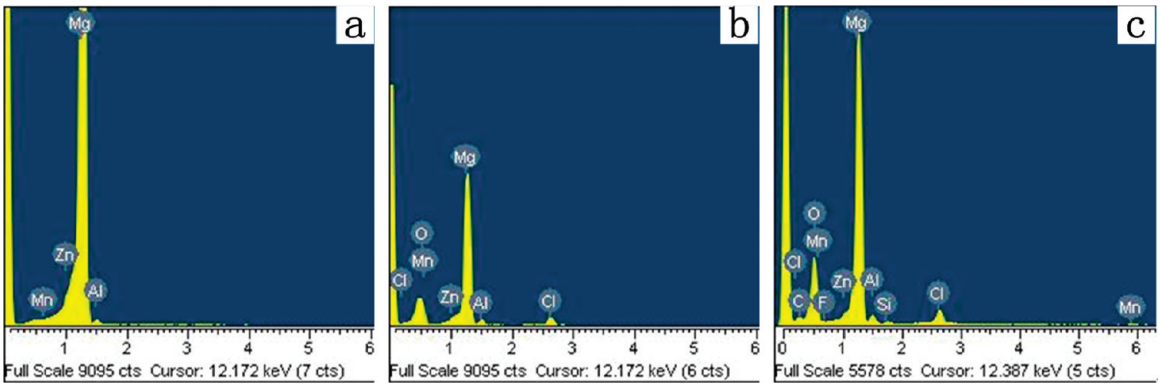

Figure 5. EDS spectra of the Mg alloy surfaces: (a) untreated Mg alloy surfaces, (b) Mg alloy surfaces treated by electrochemical machining, and (c) Mg alloy surfaces treated by electrochemical machining and FAS.

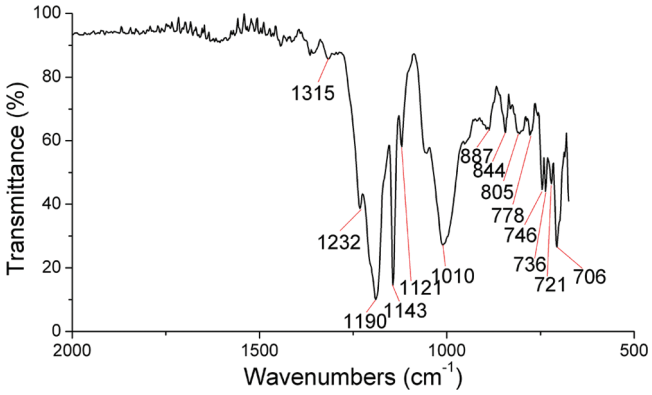

Figure 6. FTIR spectra of the Mg alloy surfaces treated by electrochemical machining and FAS.

Mg alloy surfaces, the real solid−liquid contact area is 1.17 times the projected value.

FAS, which contains the $-CF_3$ group with a surface energy of 6.7 mJ/m^2 and the $-CF_2-$ group with a surface energy of 18 mJ/m^2, was used to reduce the free energy of the Mg alloy surfaces. The self-assembly of FAS on the Mg alloy surfaces is shown in Figure 4. First, the silicon ethoxide ($Si\text{-}OC_2H_5$) functional groups react with water to form silanols (Si−OH), which act as the reactive groups at the end of the molecule. The silanols subsequently react with the −OH groups to form a self-assembled film. Meanwhile, the surface can also induce vertical polymerization to form a grafted polysiloxane.

Figure 5 shows the EDS spectra of the untreated, superhydrophilic, and superhydrophobic Mg alloy surfaces. The appearance of elemental Cl and O in Figure 4b is due to the presence of spots of $MgCl_2$ and $Mg(OH)_2$.[22] Compared to the Mg alloy surfaces treated by electrochemical machining alone, the superhydrophobic surfaces treated by electrochemical machining and FAS mainly consist of elemental Mg, Al, Zn, Mn, Cl, O, C, F, and Si, indicating that the FAS film has self-assembled on the Mg alloy surfaces.[23] Figure 6 shows the FTIR spectra of the Mg alloy surfaces treated by electrochemical machining and FAS. Five absorption bands at around 1315, 1232, 1190, 1143, and 1121 cm^{-1} are assigned to the C−F stretching vibration of the $-CF_3$ and $-CF_2-$ groups of the FAS molecules, further confirming that the self-assembly of the FAS coating on the Mg alloy surfaces.[24] FAS has a very low surface energy and can effectively reduce the free energy of the Mg alloy surfaces because of the existence of the $-CF_3$ and the $-CF_2-$ groups (6.7 and 18 mJ/m^2 surface energies, respectively).

As a conclusion, the superhydrophobicity of the Mg alloy surfaces mainly results from the presence of the hierarchical rough structures and low surface energy materials on the surface. A water droplet with a size much larger than the aforementioned microstructures does not penetrate into the grooves between the rough structures, but is rather suspended on the rough structures, resulting in heterogeneous surfaces composed of air and solids; this condition is called a Cassie−Baxter state. The contact angle in terms of the Cassie−Baxter equation is described as follows[25]

$$\cos\theta_c = f_1\cos\theta - f_2 \quad (2)$$

where θ_c and θ represent the contact angles on the FAS-modified rough and smooth surfaces, respectively, and f_1 and f_2 are the area fractions of the solid and air on the surface, respectively. Given that $f_1 + f_2 = 1$, $\theta_c = 165.2°$, and $\theta = 106.6°$, f_1 and f_2 are estimated at 0.046 and 0.954, respectively. These data indicate that when a water droplet is placed on the superhydrophobic Mg alloy surface, approximately 4.6% serves as the contact area of the water droplet and the solid surface, and the remaining 95.4% serves as the contact area of the water droplet and air. This result is better than that of Yin (90%) and Wang (85%), which were obtained on Mg alloy substrates via a chemical etching method.[9,10]

3.3. Analysis of the Hierarchical Rough Structures. The chemical compositions and organizational structures of the AZ61 Mg alloys are heterogeneous, and the Mg alloys consist of two main phases, namely, the Mg-rich α phase, and the Al-rich ($M_{17}Al_{12}$) β phase.[1] In addition, other phases and impurities composed of Mn, Zn and other trace elements are present in the interior of the AZ61 Mg alloys. The orders of anodic dissolution of the α phase and other phases or impurities under an applied electric field are different because of their different electrode potentials. Galicia et al. investigated the impedance distribution on the Mg alloy surfaces using local electrochemical impedance spectroscopy (LEIS) and found that the electrode potential of the α phase is lower than that of the β phase.[26] This finding indicates that the corrosion resistance of the α phase is poor and will result in the preferential dissolution of the α phase under an applied electric field. By contrast, the dissolution velocity of the β phase, which has a higher electrode potential, is slower than that of the α phase, and the β phase remains on the surfaces as

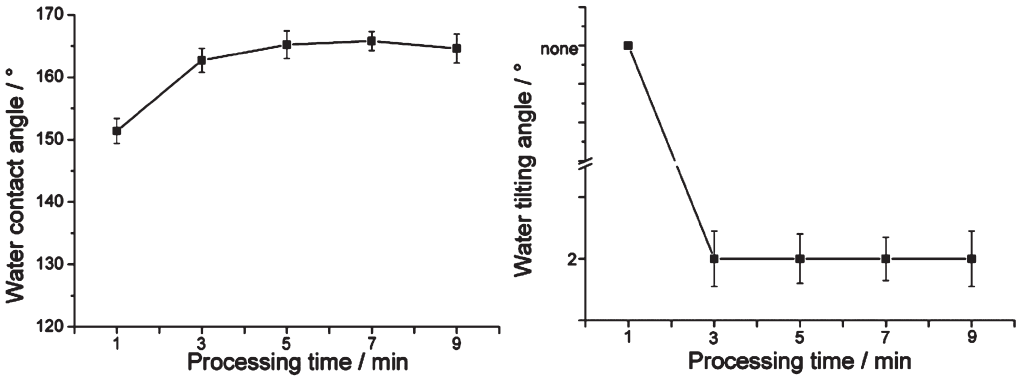

Figure 7. Variation in the water contact angles and titling angles of the sample surfaces with the processing time.

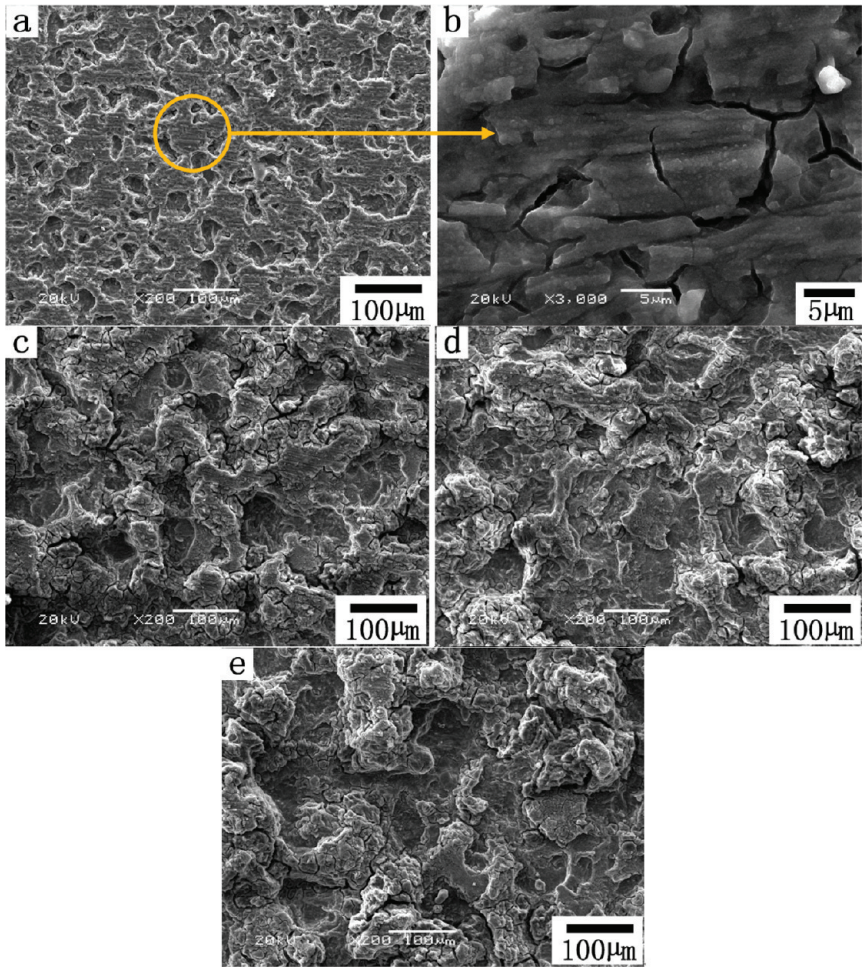

Figure 8. SEM images of the Mg alloy surfaces at different processing time: (a) 1, (c) 3, (d) 5, and (e) 7 min.

protrusions. Moreover, the other phases and impurities also remain on the AZ61 Mg alloy surfaces because of their higher electrode potentials compared with the α-Mg matrix. Song et al. investigated the dissolution of Mg and its alloys. They found that during the anodic dissolution of Mg−Al−Zn alloys, Mg was still the main component dissolving into solution, some Al also dissolved, and almost no dissolved Zn was found in the solution.[27] Song's above research further proved the preferential dissolution of the α-Mg matrix of the Mg alloys under an applied electric field.

As the processing time increases and the dissolution of the α phase in some parts of the Mg alloy surfaces proceeds, some protrusions will detach as the residues and be carried away by the electrolyte. This phenomenon is called the dissolution−abscission theory. MaKar et al. obtained an SEM image, showing that the surrounding of a particle (approximately 10 μm in diameter) on the Mg alloy surface has been dug into a hole with the dissolution of the surrounding α-Mg matrix, but the particle are still stuck in the hole.[28] This phenomenon is a strong evidence of

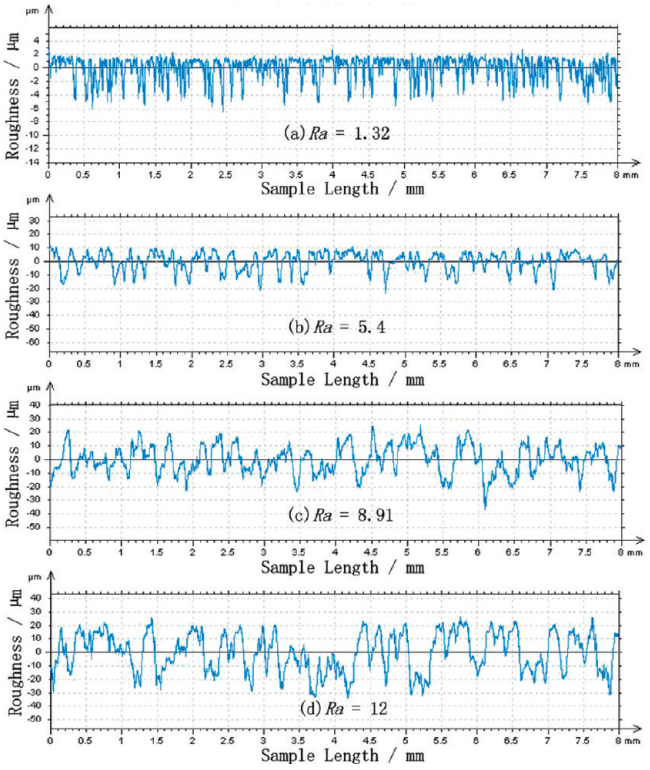

Figure 9. Surface roughness profile curves of the Mg alloy surfaces at different processing times: (a) 1, (b) 3, (c) 5, and (d) 7 min.

the rationality of the dissolution-abscission theory. However, the driving force of the dissolution of the α-Mg matrix around the aforementioned particle is simply the galvanic effect; thus, the corrosion velocity is low. The velocity of the dissolution-abscission is high in our experiment because of the high anode potential, large current density, and electrolyte flow. Song et al. pointed out that impurity particles with high electrode potentials detach from the Mg substrates because of the dissolution of the surrounding α-Mg matrix under an extremely high anode potential or current.[22]

In addition, the anodic dissolution of the Mg alloys exhibits an unexpected behavior because of the negative difference effect (NDE) corresponding to an increase in hydrogen production with increasing potential.[29] When the buoyancy is beyond the adhesion to the substrate, the hydrogen bubbles detach from the substrate surfaces and carry off corrosion products, but fill the fresh electrolyte, resulting in different corrosion velocities for the different positions.

Moreover, the solidification on the Mg alloy surfaces leads to the microsegregation of the compositions even in the internal areas of the α phase grains, which can result in different corrosion velocities in the internal of the α phase grains.

Therefore, the hierarchical rough structures are fabricated under the influence of the aforementioned factors.

3.4. Effect of the Processing Time on Wettability. To explore the effect of the processing time on wettability, the Mg alloy plates were electrochemically machined for 1, 3, 5, 7, and 9 min at the 200 mA/cm^2 processing current density. Figure 7 shows the variation in the water contact and tilting angles with the processing time. The water contact angles significantly increase within 3 min with increasing processing time. At 1 min processing time, the contact angle of the Mg alloy surfaces is 151.4° because of the increased roughness, as shown in Figure 8a and Figure 9a. However, a large uncorroded area still exists (Figure 8a); the amplified images of uncorroded area are shown in Figure 8b. The scratches generated by sanding are still present on the surface of the uncorroded area, which is larger than the area of the corrosion pits and exhibits low roughness [the roughness *Ra* is 1.32 μm, as shown in (Figure 9a)]. Thus, when the water droplet comes in contact with the Mg alloy surfaces processed in 1 min, the water droplet penetrates into the rough structures, and the tilting angle becomes so large that the water droplet still adheres to the surface even when the sample is turned over 180°. This superhydrophobic surface with high adhesion reaches the Wenzel state rather than the Cassie−Baxter state. According to eq 1, the actual solid−liquid contact area is 3.07 times the projected value. The corrosion resistance of this surface is low because of the large solid−liquid contact area, but the adhesive ability is promising for applications in no-loss water transportation.[30,31] When the processing time surpasses 3 min, the corrosion pits become larger and link together to form larger pits, as shown in Figure 8c−e. Meanwhile, relatively finer rough structures form on the pits and protrusions, leading to increased roughness of the surfaces. Surface roughness measurements show that the roughness *Ra* of the Mg alloy surfaces increases from 5.4 μm at 3 min to 8.9 μm at 5 min, and finally to 12 μm at 7 min (Figure 9b−d). Thus, the rough surfaces reach the Cassie−Baxter state, and the tilting angle of the water droplet on it is just 2° (Figure 7b). Figure 7a shows the water contact angles at 3 and 5 min processing time are 162.7 and 165.2°, respectively, indicating the higher superhydrophobicity with the processing time at 5 min.

Table 1. Processing Parameters at a Constant Removal Mass Per Unit Area

processing time (min)	processing current density(mA cm^2)	removal mass per unit area(mg/cm^2)	removal rate per unit area(mg/min cm^2)
20	50	11.13	0.56
5	200	11.10	2.22
2.5	400	11.23	4.49
1	1000	11.28	11.28

3.5. Effect of the Removal Rate Per Unit Area on the Wettability. On the basis of Faraday's laws, the metal-removal mass of the anodic surfaces is as follows[32]

$$m = \eta KIt \tag{3}$$

where m = mass of the anodic dissolution of the metal (g), η = current efficiency, K = electrochemical equivalent of the metal [g/(Ah)], I = electrochemical machining current (A), and t = electrochemical machining time (h).

The electrolyte used in the current study is the neutral NaCl aqueous solution, which is a linear electrolyte. The current efficiency η almost remains constant with the current density. When the anodic materials are constant, the electrochemical equivalent K in eq 3 is also constant. Therefore, according to eq 3, when the removal mass per unit area is constant, the processing time can be reduced by increasing the current density. A good superhydrophobicity, with a 165.2° water contact angle and 2° tilting angle, is obtained at the 200 mA/cm^2 current density and 5 min processing time, and the removal mass per unit area is 11.10 mg/cm^2. The effect of the removal rate per unit area on the superhydrophobic properties on the Mg alloy surfaces at a

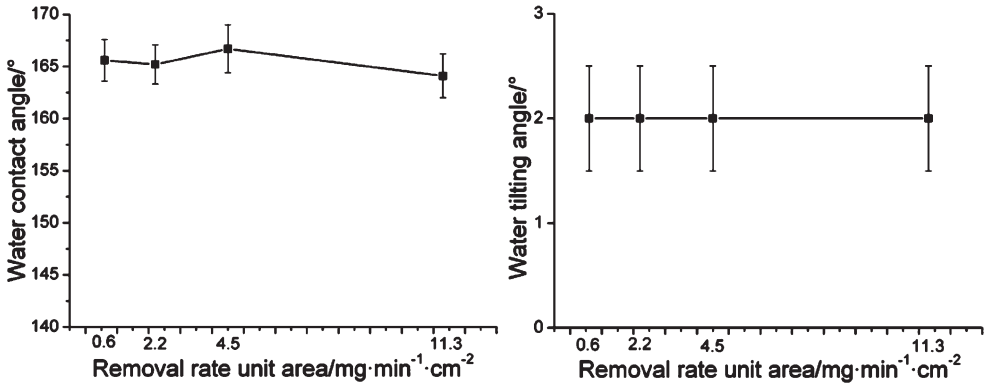

Figure 10. Variation in the water contact and tilting angles of the samples with the removal rate per unit area.

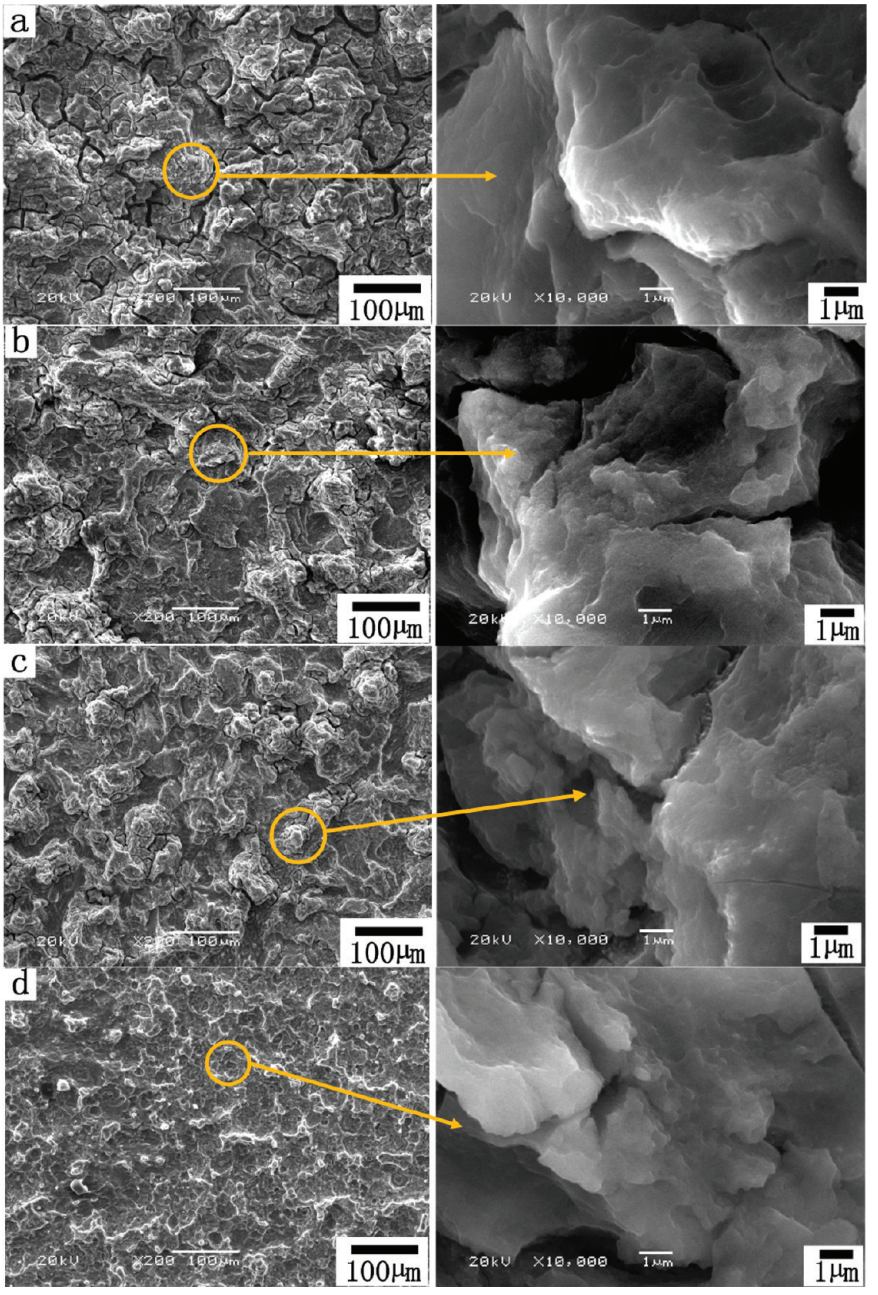

Figure 11. SEM images of the Mg alloy surfaces at different removal rates per unit area: (a) 0.56, (b) 2.22, (c) 4.49, and (d) 11.28 mg/(min cm^2).

constant removal mass per unit area was investigated; the specific parameters are shown in Table 1.

Figure 10 shows the variation in the water contact and tilting angles with the removal rate per unit area, respectively. The effect of the removal rate per unit area on the wettability of the Mg alloy surfaces is small. The water contact angles show small fluctuations with the removal rate per unit area and still reach 164.1° when the removal rate per unit area is 11.28 mg/(min cm^2). On the other hand, the removal rate per unit area has no effect on the water tilting angles. Figure 11 shows the SEM images of the Mg alloy surfaces at different removal rate per unit area. The sizes of the rough structures on Mg alloy surfaces vary with different current densities which resulting in different dissolution velocities of the α phase, different abscission velocities of the β phase, and different hydrogen evolution rates. However, the hierarchical rough structures still exist, which still meets the conditions for superhydrophobicity.

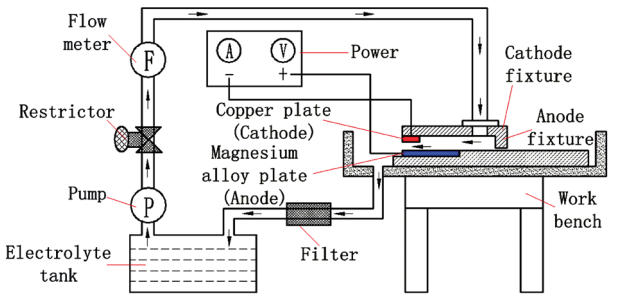

Figure 12. Experimental setup of the fabrication of the large-area superhydrophobic Mg alloy surfaces using a small-area moving cathode.

The results show that when electrochemical machining is used to fabricate the superhydrophobic Mg alloy surfaces, the processing time can be reduced and the processing efficiency can be increased by increasing the processing current density at a constant removal mass per unit area.

3.6. Fabrication of the Large-Area Mg Alloy Surfaces Using a Small Area Moving Cathode. Figure 12 shows the experimental setup of the fabrication of the superhydrophobic Mg alloy surfaces using a small-area moving cathode. Figure 13a shows the digital image of the large-area anodic Mg alloy plate (120 mm ×90 mm processing area) and a cathodic Cu plate (30 mm × 30 mm effective area). The numbers in Figure 13b represent the trajectory of the cathodic Cu plate or the processing order of the different parts of the anodic Mg alloys. These two electrodes are separated by the electrolyte at a distance of 16 mm. When an electric current passes through the electrolyte, the material on the Mg alloy surfaces facing the cathodic Cu plate dissolves, and all the Mg alloy surfaces gradually erode with the movement of the electrode. The electrolyte circulation system was used in the processing to ensure that the interval between the anode and the cathode is occupied by the electrode and to carry away the reaction products and heat using a certain pressure and flow velocity. After electrochemical machining, the large-area superhydrophilic Mg alloy surfaces were obtained. After the FAS treatment, the superhydrophilicity was easily transformed into superhydrophobicity (Figure 14).

3.7. Corrosion Resistance Performance of the Superhydrophobic Mg Alloy Surfaces. To date, the polarization curve is a useful tool in determining the instantaneous corrosion rate of a substrate. In a typical polarization curve, a lower corrosion current density or a higher corrosion potential corresponds to a lower corrosion rate and a better corrosion resistance.[8] The

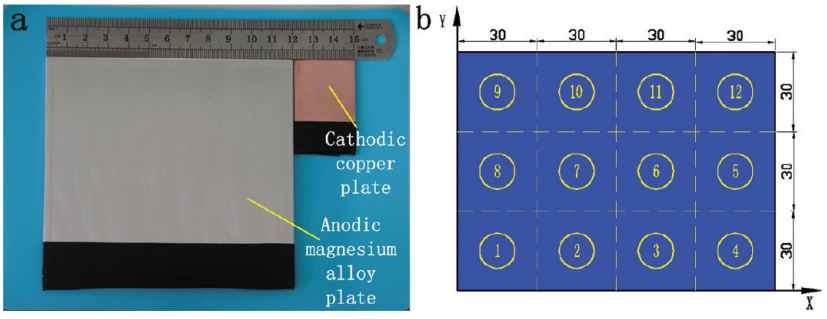

Figure 13. Digital image of the anodic Mg alloy plate and the cathodic Cu plate. (a) The effective area of the cathode is 1/12 that of the anode. (b) The numbers represent the trajectory of the cathodic Cu plate or the processing order of the different parts of the anodic Mg alloy.

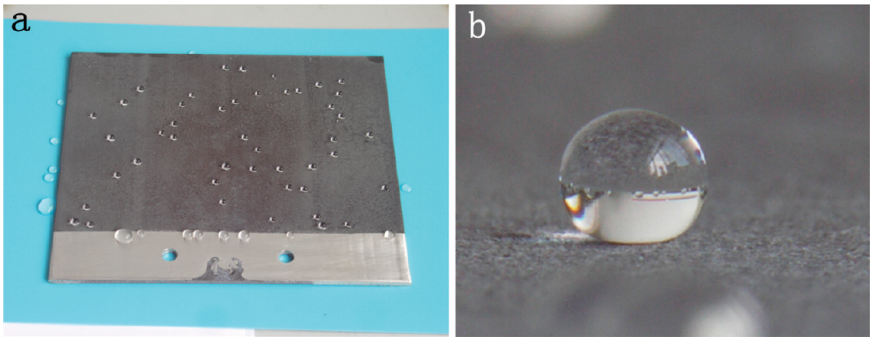

Figure 14. Digital images of (a) the large-area superhydrophobic surface, and (b) the shape of the water droplets on the superhydrophobic surface.

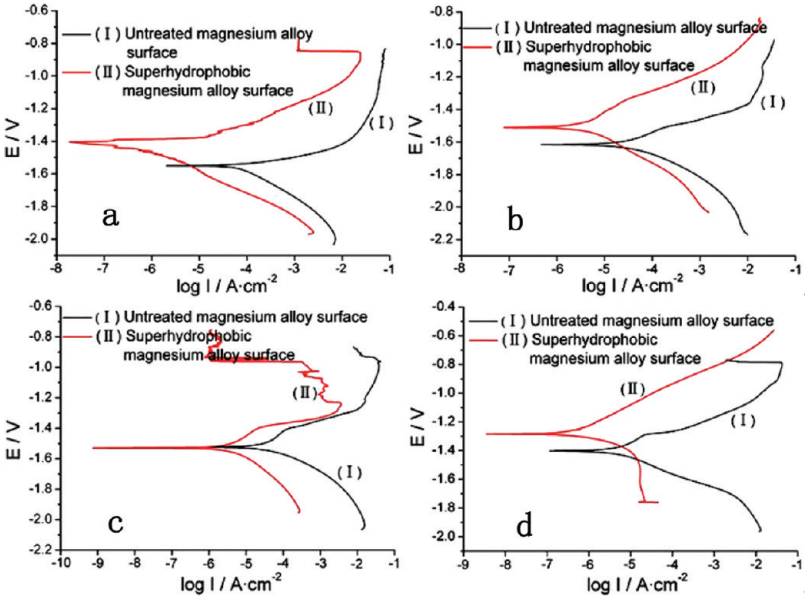

Figure 15. Potentiodynamic polarization curves of the untreated and superhydrophobic AZ61 Mg alloy surfaces in different corrosive solutions: (a) 3.5 wt % NaCl aqueous solution, (b) 3.5 wt % Na_2SO_4 aqueous solution, (c) 3.5 wt % $NaClO_3$ aqueous solution, (d) 3.5 wt % $NaNO_3$ aqueous solution.

Table 2. Corrosion Potential (E_{corr}) and Corrosion Current Density (I_{corr}) of the Untreated and Superhydrophobic Mg Alloy Surfaces in Different Corrosive Solutions

	NaCl solution		Na_2SO_4 solution		$NaClO_3$ solution		$NaNO_3$ solution	
sample	E_{corr}(V)	I_{corr}(A/cm^{-2})	E_{corr}(V)	I_{corr}(A/cm^{-2})	E_{corr}(V)	I_{corr}(A/cm^{-2})	E_{corr}(V)	I_{corr}(A/cm^{-2})
untreated Mg alloy surface	−1.5847	9.96×10^{-5}	−1.6163	4.71×10^{-7}	−1.5246	8.58×10^{-7}	−1.4029	1.15×10^{-7}
superhydrophobic Mg alloy surface	−1.4221	9.68×10^{-8}	−1.5102	7.62×10^{-8}	−1.5301	7.37×10^{-10}	−1.2845	3.51×10^{-9}

potentiodynamic polarization curves of the untreated and superhydrophobic AZ61 Mg alloy surfaces at the 200 mA/cm^2 processing current density and 5 min processing time in the different corrosive solutions were obtained using the Tafel extrapolation method and are given in Figure 15. The corrosion potential (E_{corr}) and corrosion current density (I_{corr}) derived from the potentiodynamic polarization curves are shown in Table 2. The corrosion potential (E_{corr}) of the superhydrophobic Mg alloy surface is more positive than that of the untreated Mg alloy surface, whether in the 3.5 wt % aqueous solution of NaCl, Na_2SO_4, or $NaNO_3$. The shift in E_{corr} in the positive direction may be linked to an improvement in the protective properties of the superhydrophobicity formed on the AZ61 Mg alloy surface.[2] The corrosion current densities (I_{corr}) of the untreated Mg alloy surface in the three corrosive solutions are 9.96×10^{-5}, 4.71×10^{-7}, and 1.15×10^{-7} A/cm^2, respectively, whereas those of the superhydrophobic Mg alloy surface are 9.68×10^{-8}, 7.62×10^{-8}, and 3.51×10^{-9}A/cm^2, respectively. It should be noted that the corrosion current density is reduced by more than 1 order of the Mg alloy surface after the sample acquires superhydrophobicity. Such low current density indicates an excellent corrosion resistance for the superhydrophobic Mg alloy surface. For the $NaClO_3$ corrosive aqueous solution, although the E_{corr} of the superhydrophobic Mg alloy surface is not smaller than that of the untreated Mg alloy surface, the I_{coor} of the superhydrophobic Mg alloy decreases by more than 3 orders of magnitude compared with that of the untreated magnesium alloy surface. This result indicates that the superhydrophobic Mg alloy surface has better corrosion resistance in the $NaClO_3$ aqueous solution. The electrochemical impedance spectroscopy measurements in the different corrosive solutions were also conducted to better characterize the protective behavior of the samples. Figure 16 shows that the impedance of the superhydrophobic Mg alloy surface is much higher than that of the untreated Mg alloy surface, again indicating that the superhydrophobic Mg alloy surface has good corrosion resistance.

3.8. Analysis of the Superhydrophobic Mg Alloy Surface Durability. The durability of the superhydrophobic Mg alloy surfaces is a very important factor that will determine the feasibility of the proposed method in industrial applications. The effects of the exposure time to air, pH values, and immersion time in the 3.5 wt % NaCl aqueous solution on the wettability of the superhydrophobic Mg alloy surfaces were examined. Figure 17 shows the relationship between the exposure time to air and the water contact angles of the superhydrophobic Mg alloy surfaces. All water contact angles slightly changed during air exposure for 6 months, indicating that the superhydrophobic surfaces have good long-term stability in air.

Figure 18 shows the relationship between pH and the water contact angles of the superhydrophobic Mg alloy surfaces. No obvious fluctuation in the water contact angle values within the experimental errors was observed. All static water contact angle values are in the 162.0−166.5° range, indicating that pH of the aqueous solutions have little effect on the water

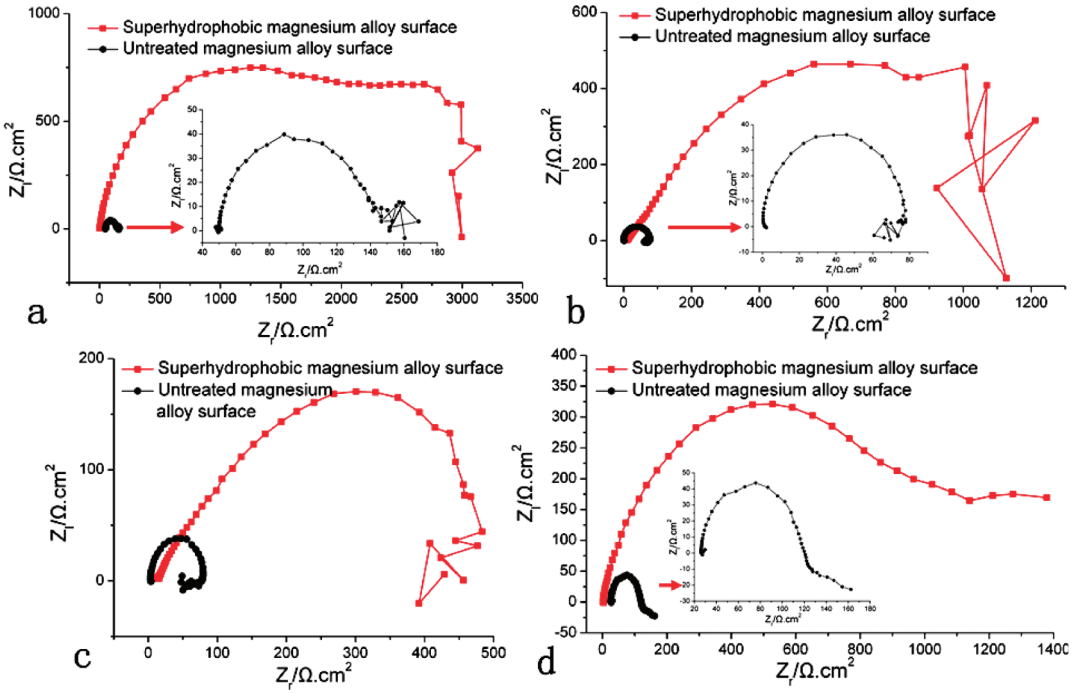

Figure 16. Nyquist plots of the untreated and superhydrophobic Mg alloy surfaces in different corrosive solutions: (a) 3.5 wt % NaCl aqueous solution, (b) 3.5 wt % Na_2SO_4 aqueous solution, (c) 3.5 wt % $NaClO_3$ aqueous solution, and (d) 3.5 wt % $NaNO_3$ aqueous solution.

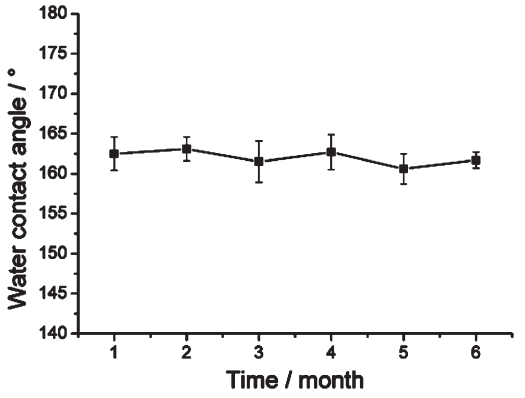

Figure 17. Water contact angles of the superhydrophobic Mg alloy surfaces after air exposure for different time.

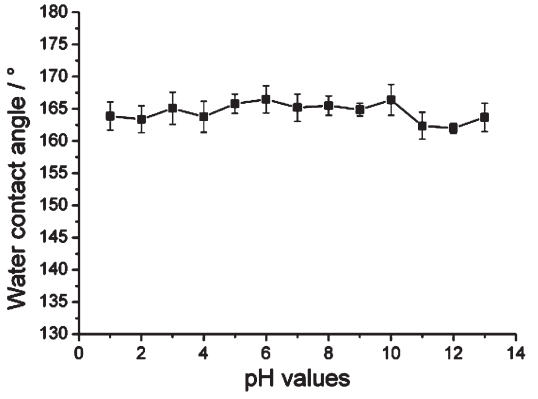

Figure 18. Relationship between pH and the water contact angles of the superhydrophobic Mg alloy surfaces.

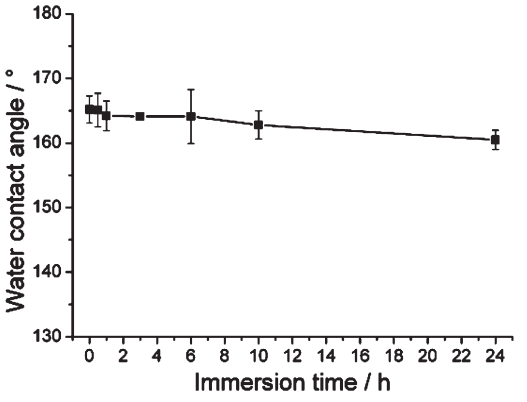

Figure 19. Changes in the water contact angles of the superhydrophobic Mg alloy surfaces as a function of the immersion time in 3.5 wt % NaCl aqueous solution.

contact angles in the resulting superhydrophobic Mg alloy surfaces.

Figure 19 shows the changes in the water contact angles of the superhydrophobic Mg alloy surfaces as a function of the immersion time in the 3.5 wt % NaCl aqueous solution. The average static water contact angles measured on the superhydrophobic surfaces gradually decrease with time. However, a contact angle of 160.5° was still obtained after 24 h immersion time, indicating good surface superhydrophobicity. This result suggests that the immersion in 3.5 wt % NaCl aqueous solution for 24 h does not induce any change in the surface states from the wettability point of view.

In conclusion, the as-fabricated superhydrophobic Mg alloy surfaces obtained using the proposed method show long-term stability in air as well as excellent resistance to corrosive liquids,

including acidic, alkaline, and salt solutions. These results are highly significant for the application of superhydrophobic Mg alloy surfaces as engineering materials.

4. CONCLUSIONS

(1) We have developed a highly effective, environmentally friendly, and nontoxic method of creating a superhydrophobic surface on an AZ61 Mg alloy substrate via an electrochemical machining method. The water contact angle of the obtained superhydrophobic surface is 165.2°, and the water tilting angle is approximately 2°.

(2) The superhydrophobicity of the Mg alloy surfaces is attributed to the combination of the hierarchical rough structures via the electrochemical machining method and the hydrophobic FAS film formed after chemical modification with FAS.

(3) The processing conditions, such as the processing time and the removal rate per unit area with a constant removal mass per unit area, were investigated to determine their effect on the wettability of the superhydrophobic surface. The water contact and tilting angles significantly increased or decreased, respectively, within 3 min with increasing processing time, respectively, and remained constant when the processing time was longer than 3 min. Moreover, when the removal mass per unit area was constant at approximately 11.10 mg/cm^2, the superhydrophobicity did not change significantly with the change in the removal rate per unit area. This observation indicates that the superhydrophobic Mg alloy surfaces can be rapidly obtained by increasing the processing current density.

(4) A large-area superhydrophobic Mg alloy surface has been successfully fabricated for the first time using a small-area moving cathode.

(5) The corrosion resistance of the superhydrophobic Mg alloy surfaces was investigated using electrochemical measurements. The findings reveal that superhydrophobic surfaces can provide a stable corrosion protection for the Mg alloys.

(6) The resulting superhydrophobic Mg alloy surfaces show long-term stability in air and excellent resistance to corrosive liquids, including acidic, alkaline, and salt solutions.

AUTHOR INFORMATION

Corresponding Author

*Tel: 86-411-84708422. Fax: 86-411-84708422. E-mail: wenjixu@dlut.edu.cn.

ACKNOWLEDGMENT

This work was financially supported by the Natural Science Foundation of China (NSFC, Grant 90923022).

REFERENCES

(1) Ballerini, G.; Bardi, U.; Bignucolo, R.; Ceraolo, G. *Corros. Sci.* **2005**, *47*, 2173–2184.
(2) Ishizaki, T.; Saito, N. *Langmuir* **2010**, *26*, 9749–9755.
(3) Song, G.; Atrens, A.; John, D. S.; Wu, X.; Nairn, J. *Corros. Sci.* **1997**, *39*, 1981–2004.
(4) Makar, G. L.; Kruger, J. *J. Electrochem. Soc.* **1990**, *137*, 414–421.
(5) Song, G.; Atrens, A.; StJohn, D.; Nairn, J.; Li, Y. *Corros. Sci.* **1997**, *39*, 855–875.
(6) Ishizaki, T.; Sakamoto, M. *Langmuir* **2011**, *27*, 2375–2381.
(7) Wang, J.; Li, D. D.; Gao, R.; Liu, Q.; Jing, X. Y.; Wang, Y. L.; He, Y.; Zhang, M. L. *Mater. Chem. Phys.* **2011**, *129*, 154–160.
(8) Wang, J.; Li, D. D.; Liu, Q.; Yin, X.; Zhang, Y.; Jing, X. Y.; Zhang, M. L. *Electrochim. Acta* **2010**, *55*, 6897–6906.
(9) Yin, B.; Fang, L.; Hu, J.; Tang, A. Q.; Wei, W. H.; He, J. *Appl. Surf. Sci.* **2010**, *257*, 1666–1671.
(10) Wang, Y. H.; Wang, W.; Zhong, L.; Wang, J.; Jiang, Q. L.; Guo, X. Y. *Appl. Surf. Sci.* **2010**, *256*, 3837–3840.
(11) Song, G. L. *Electrochem. Solid-State Lett.* **2009**, *12*, D77–D99.
(12) Song, G. L. *Surf. Coat. Technol.* **2009**, *203*, 3618–3625.
(13) Song, G. L. *Electrochim. Acta* **2010**, *55*, 2258–2268.
(14) Song, G. L. *Prog. Org. Coatings* **2011**, *70*, 252–258.
(15) Liu, T.; Cheng, S. G.; Cheng, S.; Tian, J. T.; Chang, X. T.; Yin, Y. S. *Electrochim. Acta* **2007**, *52*, 8003–8007.
(16) Liu, T.; Yin, Y. S.; Chen, S. G. *Electrochim. Acta* **2007**, *52*, 3709–3713.
(17) Chen, S. G.; Liu, T.; Yin, Y. S. *Sci. China, Ser. E: Technol. Sci.* **2008**, *51*, 975–978.
(18) Yin, Y. S.; Liu, T.; Chen, S. G.; Liu, T.; Cheng, S. *Appl. Surf. Sci.* **2008**, *255*, 2978–2984.
(19) Liang, J.; Guo, Z. G.; Fang, J.; Hao, J. C. *Chem. Lett.* **2007**, *36*, 416–417.
(20) Liu, K. S.; Zhang, M. L.; Zhai, J.; Wang, J.; Jiang, L. *Appl. Phys. Lett.* **2008**, *92*, 183103.
(21) Wenzel, R. N. *Ind. Eng. Chem.* **1936**, *28*, 988–994.
(22) Song, G. L. *Corrosion and Protection of Mg Alloys*; Chemical Industry Press: Beijing, 2006.
(23) Li, S. M.; Zhou, S. Z.; Liu, J. H. *Acta Phys. Chim. Sin.* **2009**, *25*, 2581–2589.
(24) Sarkar, D. K.; Farzaneh, M. In *Contact Angle, Wettability and Adhesion*; Mittal, K. L., Ed.; Brill Academic Publishers: Toronto, 2008; Vol. 5, p 275.
(25) Cassie, A. B. D.; Baxter, S. *Trans. Faraday Soc.* **1944**, *40*, 546–551.
(26) Galicia, G.; Pebere, N.; Tribollet, B.; Vivier, V. *Corros. Sci.* **2009**, *51*, 1789–1794.
(27) Song, G. L.; Atrens, A. *Adv. Eng. Mater.* **1999**, *1*, 11–33.
(28) Makar, G. L.; Kruger, J. *J. Electrochem. Soc.* **1990**, *137*, 414–421.
(29) Song, G. L. *Adv. Eng. Mater.* **2005**, *7*, 563–586.
(30) Xi, J. M.; Jiang, L. *Ind. Eng. Chem. Res.* **2008**, *47*, 6354–6357.
(31) Feng, L.; Zhang, Y. N.; Xi, J. M.; Zhu, Y.; Wang, N.; Xia, F.; Jiang, L. *Langmuir* **2008**, *24*, 4114–4119.
(32) Rumyantsev, E.; Davydov, A.; *Electrochemical Machining of Metals*; MIR Publishers: Moscow, 1989.